

The sediment- and soil-balance equations are solved simultaneously, requiring that each nodal soil thickness and sediment concentration is compatible with outflow from the cell. The algebraic balance equations are

$$\sum_{j=\text{up}} c_{sj} Q_{wij} - \sum_{j=\text{down}} c_{si} Q_{wij} + \frac{A_i}{8} \sum_{j=\text{down}} C_{gij} (c_{eqij} - c_{si}) = 0 \quad (7-22)$$

$$\sum_{j=1}^8 w_{ij} K_{ij} b_{\text{up}} \left( \frac{z_j - z_i}{\Delta_{ij}} \right) + A_i Q_0 \exp\left(-\frac{b_i}{b_0}\right) - \frac{A_i}{8} \sum_{j=\text{down}} C_{gij} (c_{eqij} - c_{si}) = 0 \quad (7-23)$$

where  $b_{\text{up}}$  is the upstream soil thickness. Soil thickness for each cell is solved by bisection between a minimum thickness of 0 m [0 ft] and a large maximum depth arbitrarily assumed to be 20 m [66 ft]. The equilibrium sediment concentration is found during each bisection step. Note that bisection may result in a few cells with the maximum depth in locations with strongly convergent flow, typically in washes.

The flow-routing approach works well when there are no local minima in the domain so that there is a route from every cell to the boundary. A physical local minimum cannot exist at equilibrium unless there is a physical mechanism for removing soil (e.g., wind transport). Local minima are usually artifacts of the DEM resolution because elevations are only reported to the nearest meter, and narrow features such as upstream wash channels, which are on the order of a meter wide, may not be resolved with the DEM grid. Approximately 0.5 percent of the cells in the DEM are local minima; almost all occur in wash bottoms, but a few occur along ridgetops. For these minimum cells, two preprocessing steps were performed to eliminate artificial local minima. First, a small amount of random noise (on the order of a millimeter) was added to each cell, essentially eliminating flat spots. Second, cells forming hollows were filled to create an outflow path. A number of passes were required to eliminate multicell basins.

### 7.3 Simulation Results

The soil-thickness input used for ITYM input, shown in Figure 7-3, was developed using the same 30-m [98-ft] DEM grid used for ITYM simulations. Simulations using this grid were slow to converge in wash channels; thus, the final simulation result was obtained using several intermediate simulations. Each intermediate simulation restarted using the result from the previous simulation, with control parameters occasionally adjusted at a restart to speed convergence to the appropriate equilibrium solution.

The soil distribution shown in Figure 7-3 has soil thickness that is generally between 10 and 25 cm [4 and 10 in] on ridgetops, with areas at the base of slopes thickening to more than 50 cm [20 in] at the base of sideslopes in narrow washes and larger wash bottoms exhibiting areas in excess of 10 m [33 ft]. Some of the channels have reaches that are extremely shallow or exposed, and some areas with shallow slopes (e.g., the deep soils along the eastern edge of Figure 7-3) exhibit nonphysical speckles of shallow soil amidst a generally deep soil, in part due to the relatively coarse 1-m [3.3-ft] vertical resolution of the underlying elevation grid. The soil distribution within active channels (e.g., the channels in narrow washes to the west of the Exploratory Studies Facility) and areas with strongly convergent flow also tend to exhibit speckling.

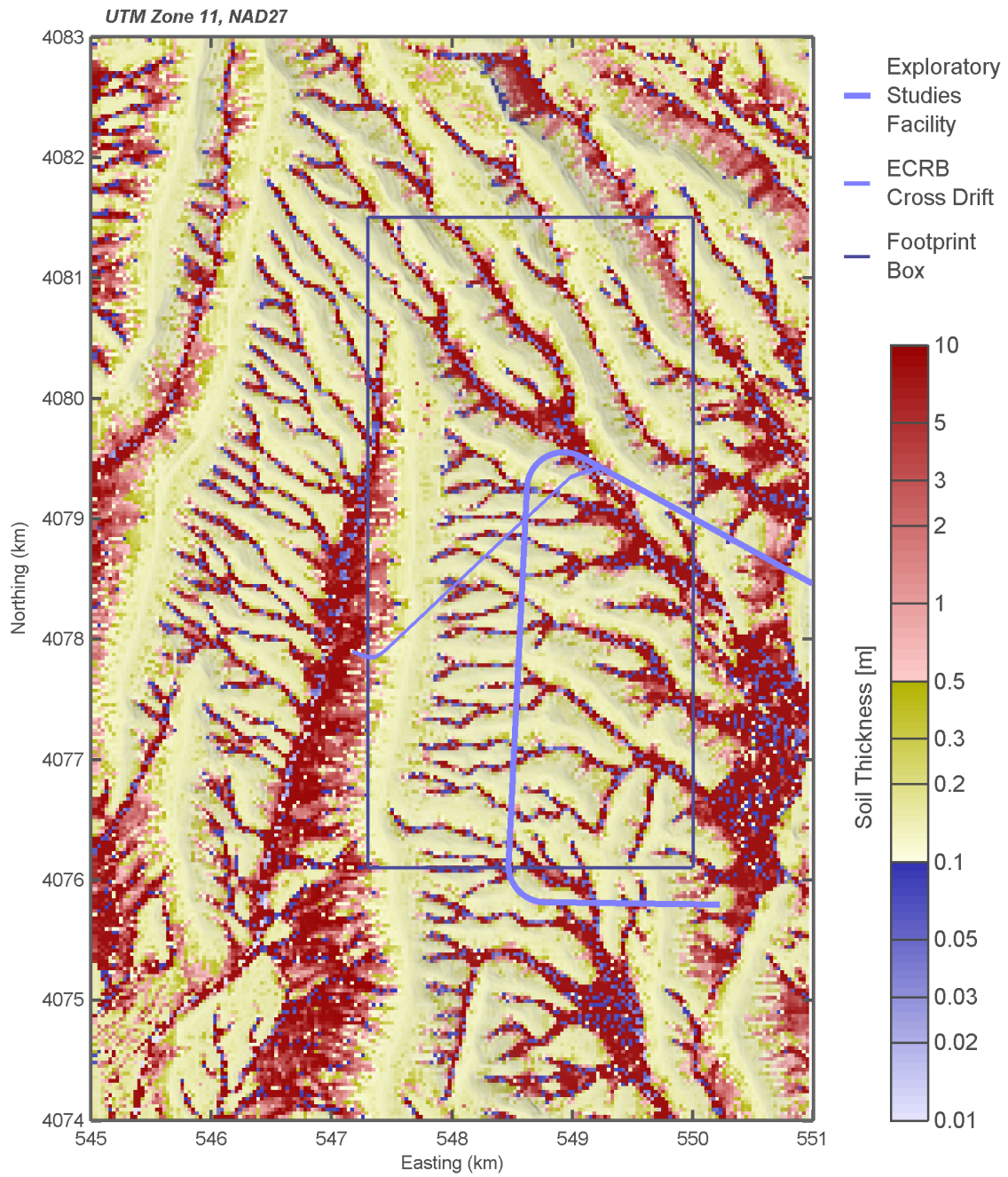


**Figure 7-3. Soil Thickness Used by Infiltration Tabulator for Yucca Mountain. Shadows Are Cast From the West Southwest. [1 m = 3.28 ft]**

The soil thickness distribution within the potential-repository footprint is thought to provide a reasonable starting point for estimating areal-average MAI, because the grid has a soil-thickness distribution representative of the site and systematic patterns across the site are described. Even the nonphysical speckling in active channels may be reasonable, because this may be the best available mechanism for considering active channels actually exposing bedrock in the narrow washes with the potential-repository footprint. The speckling does appear, however, to somewhat over-estimate the area of exposed bedrock. Note that ITYM considers the soil thickness distribution to be uncertain, with uncertainty accounted for by scaling all values by a single sampled multiplier.

Confirmatory analyses discussed in this section provide insight into the important features of the soil model. All of the confirmatory analyses use a finer grid to better represent washes and channels, extracted from a U.S. Department of Energy (DOE)-generated set of 3.1-m [10-ft] contours. The finer computational grid has cells on a 1,205 by 800 grid, with grid centers at a 7.5-m [24.6-ft] interval in both the east-west and north-south directions and a 0.3-m [1-ft] vertical resolution.

The 11 adjustable parameters in the set of coupled balance equations (and associated values) shown in Table 7-2 were found to reasonably predict soil thickness with the finer grid. Because  $F_{str}$ ,  $K$ , and  $Q_0$  control the relative importance of stream processes, soil diffusion, and weathering, these three parameters are not independent, so scaling the three parameters by the same constant does not modify the predicted soil distribution. The distributions of soil thickness and hydraulic depth shown in Figures 7-4 and 7-5, respectively, result from using the adjustable parameters in Table 7-2. A digitized outline of soil, as mapped by Scott and Bonk (1984), is shown in Figure 7-4 for reference. These distributions were generated by selecting representative parameters for the streamflow and sediment transport equations, then adjusting the soil parameters until the soil distribution was in reasonable qualitative agreement with field observations of soil thickness in trenches and other representative locations in the Yucca Mountain area.

<b>Table 7-2. Adjustable Parameters Used for Creating Soil-Thickness Distributions. Base, Low, and High Values Refer to the Reference Case and Values for Sensitivity Studies.*</b>				
<b>Parameter Name</b>	<b>Symbol</b>	<b>Base</b>	<b>Low</b>	<b>High</b>
Net rainfall rate (cm/hr)	$q_{rain}$	1	0.2	5
Manning's roughness coefficient (—)	$n$	0.2	0.05	0.8
Particle diameter (mm)	$d$	1	0.1	10
Dust deposition rate (cm/ky)	$Q_{dust}$	2.2	0.733	6.6
Alluvium creep conductance (m/s)	$K$	$10^{-11}$	$10^{-12}$	$10^{-10}$
Alluvium weathering rate ( $m^3/m^2 s$ )	$Q_0$	$10^{-13}$	$10^{-14}$	$10^{-12}$
Alluvium weathering depth (cm)	$b_0$	1	0.33	3
Fraction of time in streamflow (min/100 yr)	$F_{str}$	300	60	1,500
Kinetic coefficient during alluvium scour ( $s^{-1}$ )	$C_q$	0.1	—	—
Kinetic coefficient during bedrock scour ( $s^{-1}$ )	$C_q$	0.002	—	—
Traction coefficient for sediment equilibrium ( $s^{-1}$ )	$C_s$	$10^{-3}$	—	—
Particle specific gravity (—)	$S_s$	2.5	—	—
*1 m = 100 cm = 1,000 mm = 39.4 in				

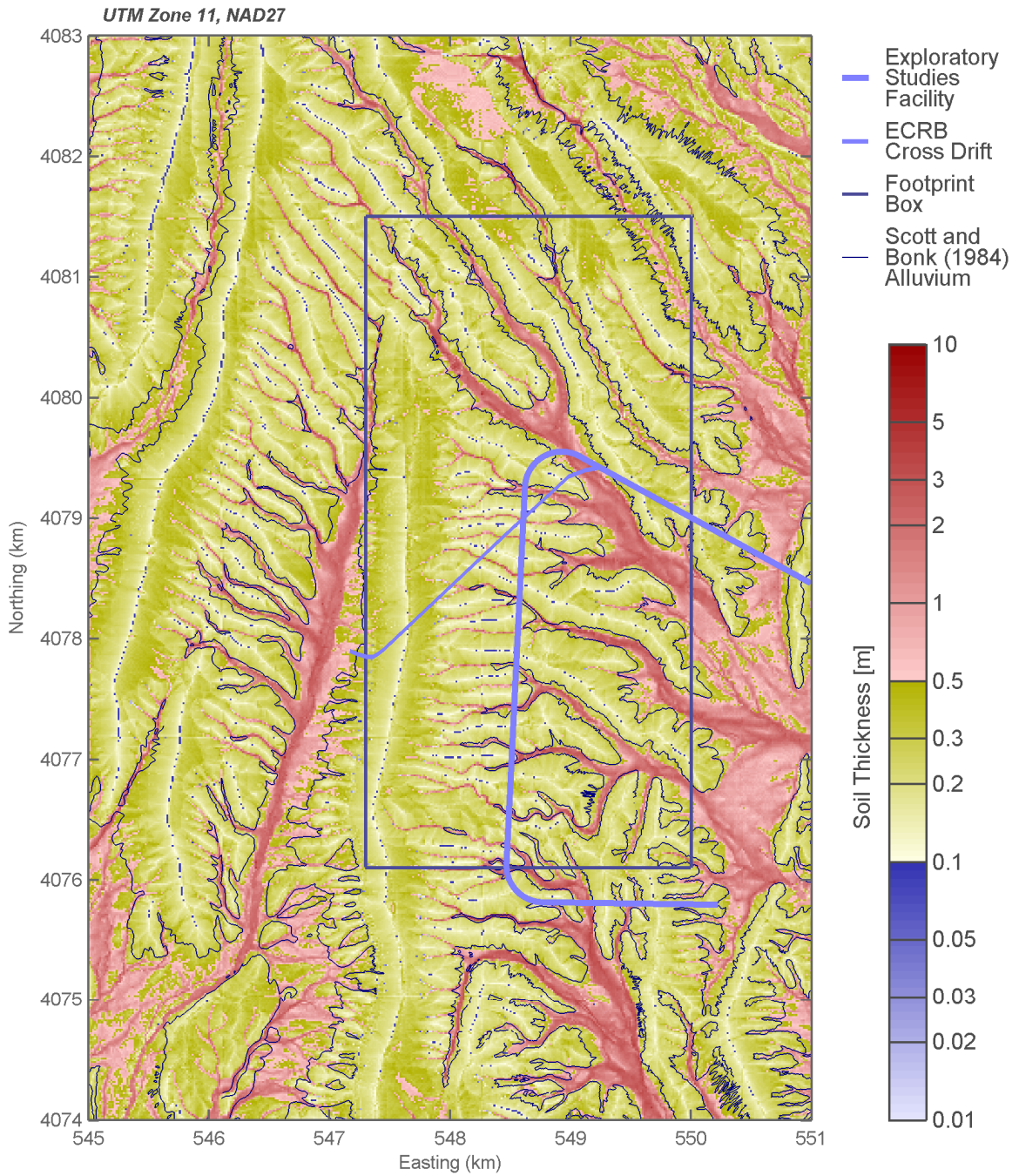


**Figure 7-4. Alluvium Thickness for the Equilibrium System Using the Parameters in Table 7-2 [1 m = 3.28 ft]**

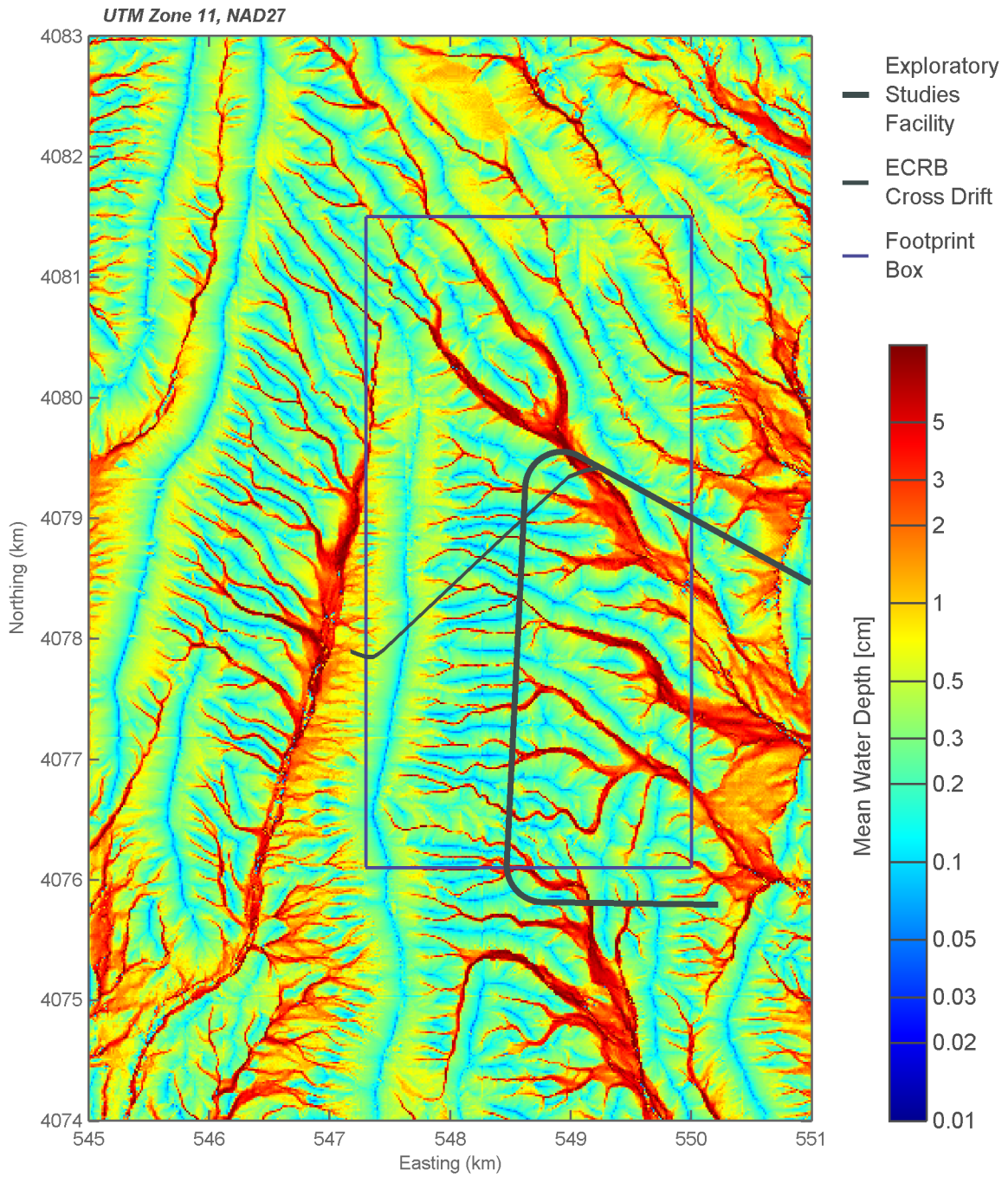


**Figure 7-5. Water Depth for the Equivalent Steady-State Storm Using the Parameters in Table 7-2 [1 cm = 0.39 in]**

A conceptual model of soil thickness has been developed based on several field expeditions to observe soil thickness using a tile probe, excavated soil pits, and open trenches and pavements (Stothoff, 2008; Fedors, 2007). The conceptual model has soil less than 10 cm [4 in] with occasional deeper pockets on the western edge of Yucca Crest, thickening to between 30 to 50 cm [12 to 20 in] downslope on shallowly dipping areas of the crest, then thinning again where slopes increase. The conceptual model has soil thickness less than 10 cm [4 in] in areas along ridgetops. Soil thickness ranges from bare to approximately 20 cm [8 in] at the top of sideslopes in the conceptual model, increasing with distance down the slope to 50 cm [20 in] or more. Observed fill thickness in the wash bottoms west of the Exploratory Studies Facility range from bare-rock to terraces several meters thick. Soil thickness was observed to vary by 20 cm [8 in] or more over distances of less than 1 m [3.3 ft].

The soil distribution illustrated in Figure 7-4 is in general accordance with the conceptual model. The model predicts average thicknesses that may be somewhat too large along crestlines and somewhat too shallow near the bottom of some of the side slopes. Areas with strongly converging flow or channels feature very shallow and deep thicknesses in adjacent cells, which appear to be numerical artifacts related to the large grid cell dimensions and relatively coarse 1-m [3.3-ft] vertical resolution. These artifacts are also related to the inherent dynamism of sediment transport processes in the deeper soil. Surface elevations vary over time as incised channels move around within deep soil, and calculations based on equilibrium physics are likely affected when using a snapshot of such dynamic topography.

Bare-rock patches in the field are local features, such as upland channels, that are smaller than a grid cell, but the calculated soil thickness values are retained outside of the Scott and Bonk (1984) alluvium outline to approximately represent the area fraction of such patches in calculating infiltration. Within the mapped soil outline, however, a postprocessing step is performed to provide more representative soil thickness. A power-law relationship of soil thickness to surface slope was determined by regression

$$\ln b = a_1 + a_2 \ln s \quad (7-24)$$

where  $s$  is the slope, in degrees, of the ground surface interpolated from the nearest four grid points in the DEM. Depth of soil cover is obtained from geologic logs and sources such as Fernandez, et al. (1994) and Flint and Flint (1995). Boreholes with reported depth of soil cover less than 1 m [3.3 ft] or slopes greater than  $25^\circ$  are not used. The selected boreholes can be conveniently grouped into 28 alluvium boreholes, which lie in alluvium or colluvium but not within an active channel, and 9 channel boreholes, which lie within active channels. Regressed coefficients are significantly different for the two groups. Figure 7-6 shows the observed soil thicknesses and regressions for the two groups.

Wherever the slope is less than  $10^\circ$  within the Scott and Bonk (1984) soil outline, the soil-routing model estimates are replaced with the soil thickness calculated using the regression equation; otherwise, the soil-routing model predictions are used. The effect of postprocessing is shown in Figure 7-7; this postprocessed distribution is directly comparable to the soil distribution in Figure 7-3 used by ITYM.

The finer grid yields a soil distribution that is more nuanced than the ITYM distribution. The ridges and hillslopes tend to have a wider range of soil thickness and somewhat deeper soil with the finer grid, and soil thickness responds more to slope. The finer grid also represents the washes and channels without the large oscillations seen in the ITYM distribution, with speckling

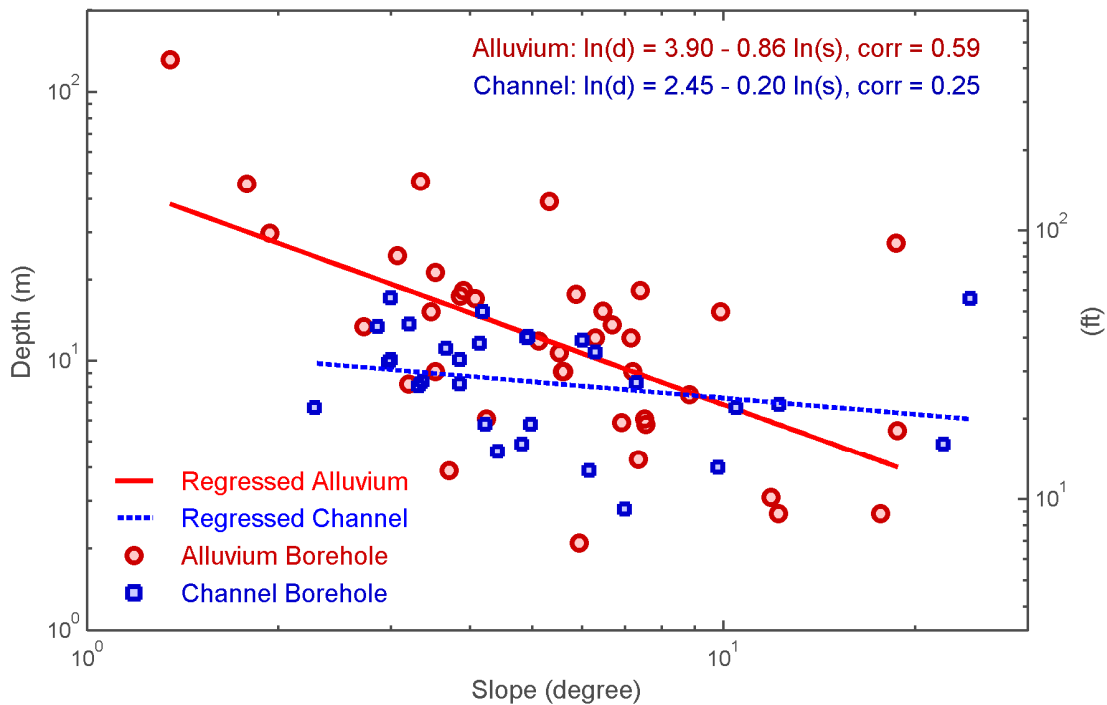


**Figure 7-6. Comparison of Regression Equation for Soil Thickness With Observations for Both Deep Alluvium and Channels [1 m = 3.28 ft]**

generally limited to the extreme headwaters of the first-order washes. The finer grid captures staff understanding of how soil thickness patterns vary with topographic position better than the ITYM distribution, although the soil thickness may be somewhat too large on ridgetops and somewhat too small at the base of sideslopes.

This soil distribution has not been upscaled into the 30-m [98-ft] grid cells used by ITYM. Upscaling using a harmonic mean is anticipated to better represent the effect of soil thickness on MAI than simply using the arithmetic mean, because the shallow-soil abstractions for MAI depend on the logarithm of soil thickness.

## 7.4 Sensitivity to Input Parameters

The calculated distribution of soil thickness depends on the input parameters in a nonlinear way. Several of the most important factors are examined in this section to evaluate sensitivity of the soil thickness distribution to the parameters as well as to evaluate the appropriate range for the parameters. The Split Wash watershed is used as a basis for comparing different simulations, because fieldwork has provided a feel for appropriate soil thickness distributions in this watershed and the scale is fine enough to see subtle differences between distributions. Note that Split Wash has also been used for detailed watershed-scale overland-flow modeling (Woolhiser, et al., 2006).

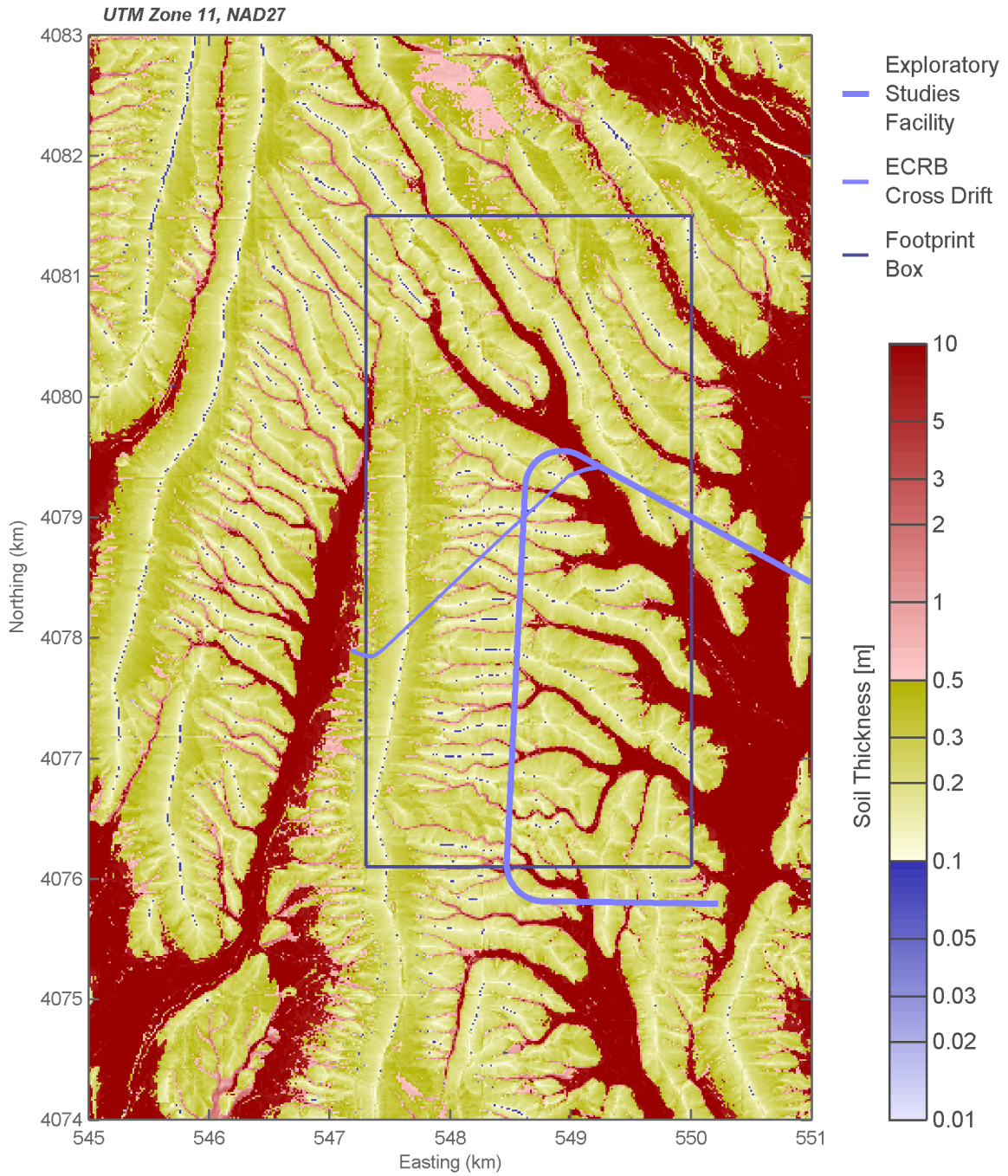


**Figure 7-7. Alluvium Thickness for the Equilibrium System Incorporating the Deep Alluvium Regression Equation [1 m = 3.28 ft]**

The DEM that ITYM uses to describe the Yucca Mountain area is at a resolution of 30 m [98.4 ft] on a side. Fine features such as first-order channels (e.g., approximately a meter wide) are not resolved with this grid. The sensitivity analysis of the soil-thickness model performed in this section uses a more highly refined grid to illustrate model sensitivities. The fine-scale computational grid described in Section 7.3, with 7.5-m [24.6-ft] grid centers, represent the coarsest scale used for the sensitivity study. Increasingly refined grids were obtained by subdividing each grid cell into 4 and 16 subcells, using bilinear interpolation to project elevations into the subcells. The finest grid cell is 1.875 m [6.15 ft] on a side, beginning to approach the resolution required to capture first-order channels (although the bedrock resolution is still at the undivided scale). All simulations in this section use the single-refinement grid, with 3.75-m [12.3-ft] cell dimensions, unless otherwise specified. The single-refinement grid is termed the base grid.

Diffusive soil flux is estimated using

$$q = -\frac{\rho K b^3}{\mu} \nabla z_s \quad (7-25)$$

where  $z_s$  is the elevation of the soil surface. The gradient of the soil surface is used to define the slope. The elevation DEM actually defines the top of the soil, but because of the possibility for inconsistencies, such as local hollows, it is more robust to use the DEM as the bedrock base and build soils above this base. The more robust technique is used in all simulations reported here. Typically, the soils are thin relative to the DEM elevation resolution, so it makes little difference whether the DEM describes the soil surface or the bedrock surface. Channels may have sufficiently thick soil, however, that the difference in elevations significantly affects soil thickness patterns.

Because the soil surface is unknown *a priori*, iteration is necessary to update downslope elevations. Each simulation discussed here uses 30 iterations to estimate soil thickness, terminating early if mean change within an iteration,  $\Delta$ , is less than 1 cm [0.4 in]. Mean change after 30 iterations is typically less than 5 cm [2 in]. Mean change is calculated by

$$\Delta = \left[ \frac{1}{N} \sum (b^{i+1} - b^i)^2 \right]^{1/2} \quad (7-26)$$

where  $b^{i+1}$  and  $b^i$  represent soil thickness from two successive iterations and there are  $N$  grid cells in the domain.

In the first iteration, the soil thickness distribution calculated from the elevation DEM provides the first estimate of the thickness distribution. In subsequent iterations, large oscillations in soil thickness occur within channels due to the cubic dependence of flux on thickness (ridgetops and hillslopes converge quickly and are essentially unaffected by oscillations). Note that the computational oscillations reflect the dynamic nature of the physical system, because the channel may move around considerably within alluvium-filled wash bottoms, actively cutting, depositing, and changing slope. To reduce channel oscillations and speed convergence to an equilibrium, soil thicknesses are only updated by a fraction of the calculated increment for all iterations after the first. Updated thickness is calculated by

$$b^{i+1} = b^i + \alpha_b (b^{i+1} - b^i) \quad (7-27)$$

where  $b^{i+1}$  is the raw thickness calculated using the most recent soil distribution,  $b^{i+1}$  is the updated thickness used in subsequent calculations, and  $\alpha_b$  is a weighting parameter (0.2 is used in calculations).

The first set of simulations demonstrates the effect of grid refinement. Each simulation uses the same base physical parameters listed in Table 7-2, which provide soil distributions that are representative of observed distributions. The three grids have cell dimensions of 7.5, 3.75, and 1.875 m [24.6, 12.3, and 6.15 ft]. The resulting soil-thickness distributions are shown in Figure 7-8, color-coded according to the soil thickness. The identical soil-thickness distribution, color-coded according to the base-10 logarithm of the soil thickness, is shown in Figure 7-9. The logarithmic scale is used in the following figures because the thickness of shallow soil is more readily identified.

Hillslope soil-thickness patterns are preserved under grid refinement, but convergent features such as channels are thinner, and wash bottoms tend to have shallower soils. The north-south discontinuity in the middle of the domain, visible in each refinement level, is an artifact that probably arose from a seam between adjacent scenes when creating the original DOE DEM used to create the contours. Features (both physical, such as small channels, and nonphysical, such as speckling) can be observed with the finer grids that are less visible in the coarse grid. Speckling (adjacent patterns of shallow and deep soils) occurs when diffusive processes are small relative to advective processes, such as on steep slopes, and may be partially because DEM errors are amplified.

The effects of different physical parameters on soil thickness are shown in Figures 7-10 through 7-15. Each parameter is investigated by multiplying and dividing the parameter by a constant factor while holding all other parameters at the base value listed in Table 7-2. The grid cells have 3.75-m [12.3-ft] sides for all simulations in Figures 7-10 through 7-15.

Effective soil conductivity mediates the relative importance of creep. When conductivity is increased (viscosity is decreased), soil thickness decreases. To maintain the same flux, a factor of eight change in effective soil conductivity should affect soil thickness by approximately a factor of two, consistent with the results shown in Figure 7-10.

The basecase scenario is not dominated by overland flow, but increases in effective-storm strength (Figure 7-11) or reductions in Manning  $n$  (Figure 7-12) move the system toward a more erosive situation. Portions of the hillslopes are stripped in the more erosive scenario for both parameters. On the other hand, the less erosive scenario is similar to the basecase for both parameters. Interestingly, the fraction of time in which overland flow occurs (Figure 7-13) has much less effect on soil-thickness distributions compared to effective storm strength or Manning's  $n$ . The effective soil particle dimension (Figure 7-14) also has little influence.

Dust is far more significant as a source material in the basecase than is bedrock. Changing the dust strength by a factor of three has a noticeable effect on distributions (Figure 7-15), but changing the bedrock source strength only affects the shallow soils on ridgetops (not shown). The variability of dust deposition rates over the last glacial cycle estimated from the Reheis, et al. (1995) data implies that, all else being equal, equilibrium hillslope and ridgetop soil thicknesses may have varied significantly over that period.

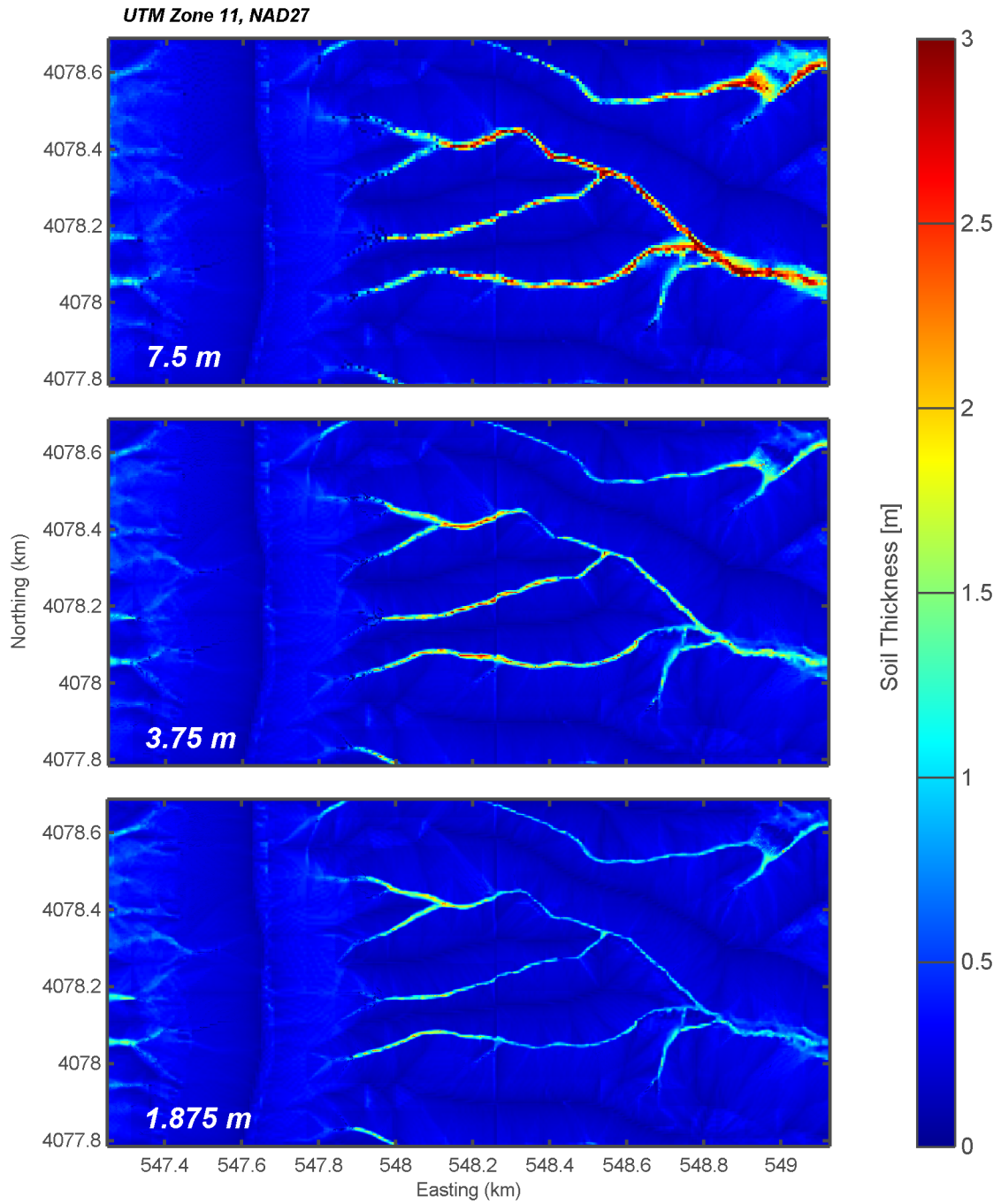


**Figure 7-8. Soil Thickness in Split Wash, Shown in a Linear Scale, for the Equilibrium System With Three Different Computational Grid Resolutions [1 m = 3.28 ft]**

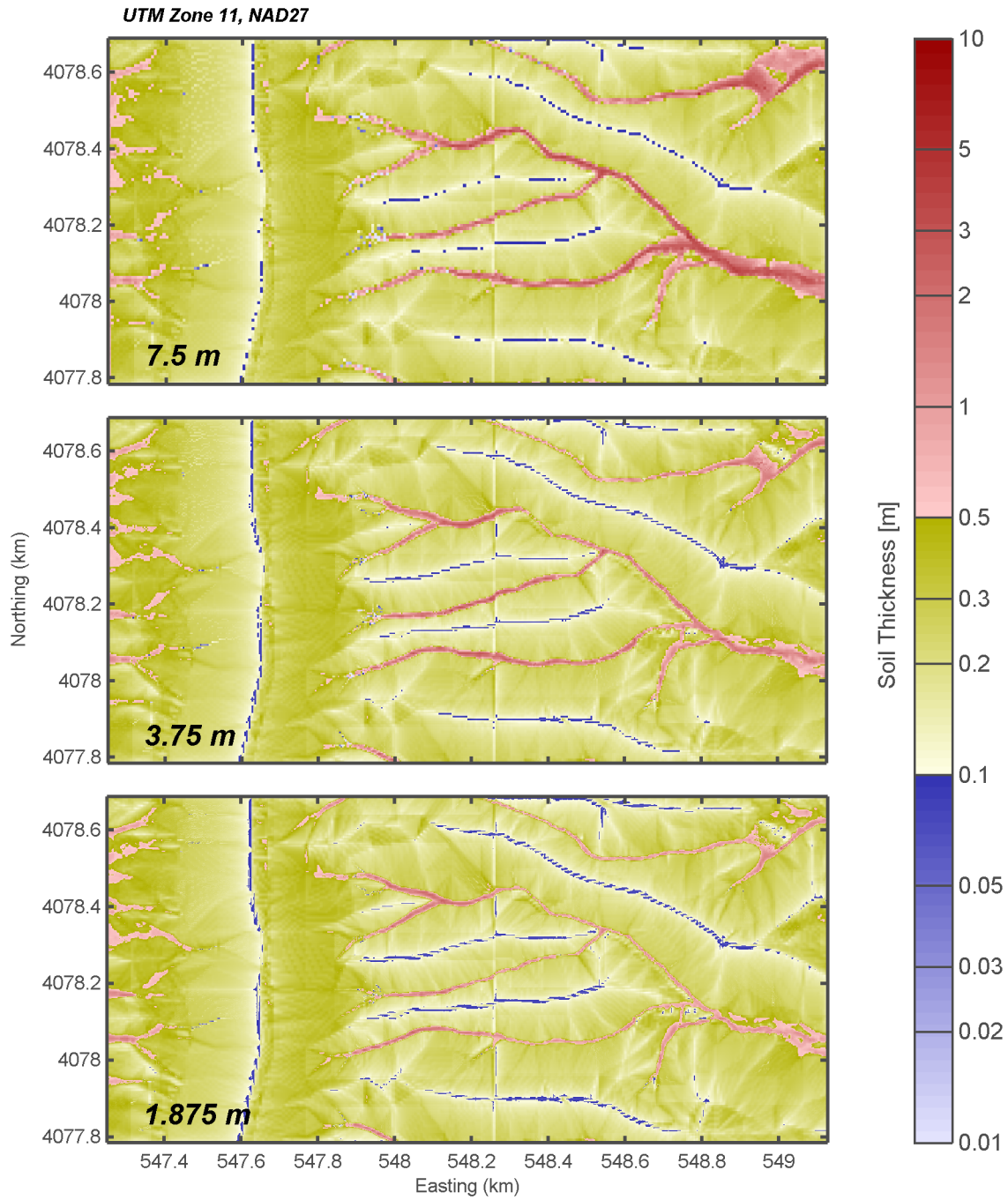


**Figure 7-9. Soil Thickness in Split Wash, Shown in a Logarithmic Scale, for the Equilibrium System With Three Different Computational Grid Resolutions [1 m = 3.28 ft]**